Pronounced zonal heterogeneity in Eocene southern high-latitude sea surface temperatures

Peter M. J. Douglas[a,1,2], Hagit P. Affek[a], Linda C. Ivany[b], Alexander J. P. Houben[c,3], Willem P. Sijp[d], Appy Sluijs[c], Stefan Schouten[c,e], and Mark Pagani[a]

[a]Department of Geology and Geophysics, Yale University, New Haven, CT 06520; [b]Department of Earth Sciences, Syracuse University, Syracuse, NY 13244; [c]Department of Earth Sciences, Faculty of Geosciences, Utrecht University, 3584 CD, Utrecht, The Netherlands; [d]Climate Change Research Centre, University of New South Wales, Sydney, NSW 2052, Australia; and [e]Department of Marine Organic Biogeochemistry, Royal Netherlands Institute for Sea Research, 1790 AB Den Burg, Texel, The Netherlands

Edited by Mark H. Thiemens, University of California, San Diego, La Jolla, CA, and approved March 21, 2014 (received for review November 15, 2013)

Paleoclimate studies suggest that increased global warmth during the Eocene epoch was greatly amplified at high latitudes, a state that climate models cannot fully reproduce. However, proxy estimates of Eocene near-Antarctic sea surface temperatures (SSTs) have produced widely divergent results at similar latitudes, with SSTs above 20 °C in the southwest Pacific contrasting with SSTs between 5 and 15 °C in the South Atlantic. Validation of this zonal temperature difference has been impeded by uncertainties inherent to the individual paleotemperature proxies applied at these sites. Here, we present multiproxy data from Seymour Island, near the Antarctic Peninsula, that provides well-constrained evidence for annual SSTs of 10–17 °C (1σ SD) during the middle and late Eocene. Comparison of the same paleotemperature proxy at Seymour Island and at the East Tasman Plateau indicate the presence of a large and consistent middle-to-late Eocene SST gradient of ∼7 °C between these two sites located at similar paleolatitudes. Intermediate-complexity climate model simulations suggest that enhanced oceanic heat transport in the South Pacific, driven by deep-water formation in the Ross Sea, was largely responsible for the observed SST gradient. These results indicate that very warm SSTs, in excess of 18 °C, did not extend uniformly across the Eocene southern high latitudes, and suggest that thermohaline circulation may partially control the distribution of high-latitude ocean temperatures in greenhouse climates. The pronounced zonal SST heterogeneity evident in the Eocene cautions against inferring past meridional temperature gradients using spatially limited data within given latitudinal bands.

paleooceanography | clumped isotopes | organic geochemistry | climate modeling | high-latitude climate

The greenhouse climates of the Eocene provide an important analog for understanding climate responses to elevated greenhouse gas concentrations (1). Current efforts to simulate Eocene climates, however, cannot reproduce geochemical evidence for very warm high-latitude temperatures and greatly reduced meridional temperature gradients (2–4). This data–model discrepancy could imply that current climate models do not adequately incorporate important high-latitude climate feedbacks (5, 6), limiting their ability to simulate polar amplification of greenhouse warming. It is also possible, however, that the available high-latitude paleotemperature proxy records are inaccurate (3), or are not representative of high-latitude temperatures generally.

Widely differing paleotemperature estimates from the southern high latitudes have complicated comparisons of paleotemperature data to models of Eocene climate. Paleotemperature estimates from the East Tasman Plateau [Ocean Drilling Program (ODP) site 1172; 67°S paleolatitude] (7) and New Zealand (55°S) (8) in the southwest Pacific (Fig. 1), derived primarily from the archaeal-lipid–based paleotemperature proxy TEX_{86} (9), yield elevated sea surface temperature (SST) estimates of 26–28 °C in the early Eocene and 17–24 °C in the middle Eocene (4) that suggest extreme polar amplification of greenhouse warmth. For comparison, modern mean annual SST at an equivalent latitude and longitude is 0 °C (10). This evidence for a tropical-to-subtropical climate in the southern high latitudes sharply contrasts with much cooler SST estimates (10–15 °C in the early Eocene; 5–15 °C in the middle Eocene) derived from bivalve oxygen isotope values ($\delta^{18}O$), from Seymour Island (∼67°S) (11, 12), offshore of the Antarctic Peninsula in the South Atlantic (Fig. 1). These temperature differences could indicate the presence of large zonal SST gradients in the Eocene southern high latitudes, with potential implications for heat transport to high latitudes in greenhouse climates.

However, there are important uncertainties in TEX_{86} temperature estimates due to multiple temperature calibrations (9) and unresolved questions regarding the provenance of sedimentary archaeal lipids (13, 14). Furthermore, bivalve $\delta^{18}O$ paleotemperatures depend on assumptions for the oxygen isotopic composition of seawater (11). Uncertainty in the age of Seymour Island sediments also complicates the comparison with other paleoclimate datasets (11), although this age uncertainty is unlikely to account for the observed temperature differences. These uncertainties in the proxy datasets have made it difficult to determine whether apparent SST differences between the southwest Pacific and South Atlantic are due to true zonal SST variability.

We performed clumped isotope analyses of the bivalve shells previously analyzed for $\delta^{18}O$ to better constrain SST estimates

Significance

Reconstructions of ancient high-latitude climates can help to constrain the amplification of global warming in polar environments. Climate models cannot reproduce the elevated high-latitude temperature estimates in the Eocene epoch, possibly indicating problems in simulating polar climate change. Widely divergent near-Antarctic Eocene sea surface temperature (SST) estimates, however, question the evidence for extreme warmth. Our analysis of multiple temperature proxies near the Antarctic Peninsula improves intersite comparisons and indicates a substantial zonal SST gradient between the southwest Pacific and South Atlantic. Simulations of Eocene ocean temperatures imply that the formation of deep water in the southwest Pacific partly accounts for this SST gradient, suggesting that climate models underestimate Eocene SSTs in regions where the thermohaline circulation leads to relatively high temperatures.

Author contributions: P.M.J.D., H.P.A., and L.C.I. designed research; P.M.J.D., A.J.P.H., and W.P.S. performed research; P.M.J.D., H.P.A., L.C.I., A.J.P.H., W.P.S., A.S., S.S., and M.P. analyzed data; and P.M.J.D. wrote the paper.

The authors declare no conflict of interest.

This article is a PNAS Direct Submission.

[1]Present address: Division of Geological and Planetary Sciences, California Institute of Technology, Pasadena, CA 91125.

[2]To whom correspondence should be addressed. E-mail: pdouglas@caltech.edu.

[3]Present address: Netherlands Organization for Applied Scientific Research (TNO), Princetonlaan 6, 3584 CB, Utrecht, The Netherlands.

This article contains supporting information online at www.pnas.org/lookup/suppl/doi:10.1073/pnas.1321441111/-/DCSupplemental.

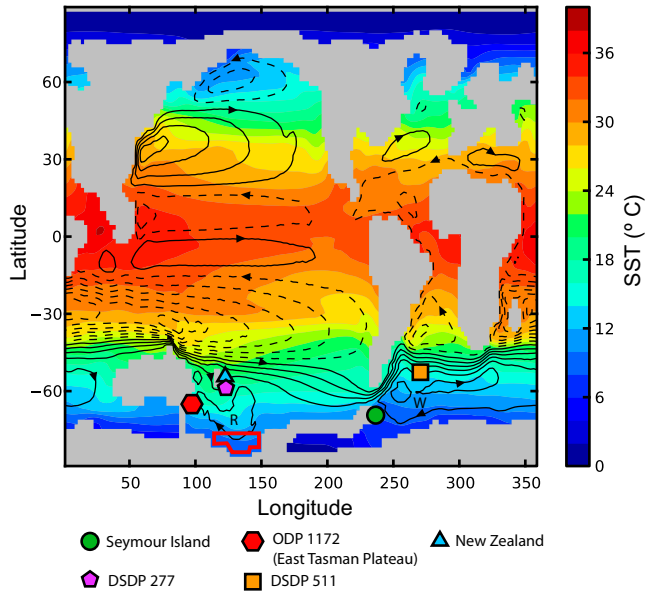

Fig. 1. The Eocene locations of SST proxy sites discussed in the text, shown with the UVic model Eocene paleogeography and sea surface temperatures from a model simulation with 1,600 ppm pCO_2. The modeled region of deep-water formation in the Ross Sea is outlined in red. The modeled depth-integrated stream function is also shown; solid and dashed lines indicate clockwise and counter clockwise flow paths, respectively. The proto-Ross and proto-Weddell gyres are labeled with an R and a W, respectively.

for Seymour Island. Carbonate clumped isotope thermometry is based on the temperature dependence of the abundance of ^{18}O—^{13}C bonds (Δ_{47}) (15), and is independent of the isotopic composition of the water from which carbonate precipitates. We also conducted TEX_{86} analyses in sediment associated with the sampled bivalve shells, to facilitate a direct comparison of SST estimates between Seymour Island and other southern high-latitude sites (7, 8, 16). To improve the chronology of these paleoclimate records we produced a new dinoflagellate cyst biostratigraphic age model for the Seymour Island La Meseta Formation. Lastly, we compared paleotemperature data from Seymour Island and other sites in the southern high latitudes with a set of intermediate-complexity climate model simulations to assess mechanisms that could have controlled the observed distribution of paleo-SSTs.

Results and Discussion

Biostratigraphic Age Model. We applied the magnetostratigraphically calibrated organic-walled dinoflagellate cyst biostratigraphic framework for the early Paleogene of the Southern Ocean (17), which is magnetostratigraphically calibrated to the 2012 geologic timescale (18), to develop a biostratigraphic age model for the Seymour Island La Meseta Formation (Fm.) (Fig. S1). This age model indicates that the La Meseta Fm. was deposited between 45 and 34 Ma (*SI Text*), contrary to previous suggestions that the formation also spanned the early Eocene (11, 12). The assignment of the lowermost sediments to an age of ~45 Ma is based on two pieces of evidence (Table S1). First, the first occurrence of *Enneadocysta diktyostila*, which is dominant in these sediments, has been calibrated to Chron C20r (~45 Ma) (19, 20). Second, essentially all taxa present in these sediments belong to the so-called transantarctic fauna, whose dominance reflects an age near the early–middle Eocene boundary (~49 Ma or younger) (21). Dinocyst assemblages in upper-stratigraphic horizons are consistent with ages between 41 and 34 Ma, as determined by the strong agreement between bivalve strontium-isotope ratios and the global seawater strontium isotope curve (11, 22).

Test of the Δ_{47}–Temperature Relationship in Bivalves. Analyses of modern coastal bivalve shells (Table S2) agree with a synthetic calcite Δ_{47}–temperature calibration that was developed using identical methods and equipment (Fig. 2) (23), supporting previous findings (24, 25) that the relationship between molluscan carbonate growth temperature and Δ_{47} agrees with inorganic calcite calibration data. Some recently published clumped isotope analyses of modern bivalve shells have suggested the possibility of significant deviations from the synthetic-calcite calibration (26–28). The reason for these deviations is unknown at present, but is likely to be at least in part due to interlaboratory methodological differences, possibly related to the temperature of acid digestion (28). The modern bivalve Δ_{47} data presented here (Fig. 2) are more relevant to our fossil samples than the datasets of refs. 27 and 28, because (*i*) those studies were conducted with a 90 °C common acid bath, while we use the same methodology as the synthetic-calcite calibration (15, 23); and (*ii*) in addition to shallow marine bivalves, the datasets of refs. 27 and 28 include cultured bivalves, deep-water bivalves, and other mollusk taxa that may exhibit different isotopic behavior.

Diagenetic Alteration of La Meseta Fm. Bivalve Shells. La Meseta Fm. bivalve fossils have been previously tested extensively for diagenetic recrystallization (11, 12, 31), including analyses of mineralogy, microstructure, minor and trace elements, and cathodoluminescence. Furthermore, growth layers with interannual and seasonal variations in $\delta^{18}O$ and $\delta^{13}C$ values are found in the shells of both the taxa studied here, suggesting that the isotopic composition of the shell carbonate has not been diagenetically reset by dissolution and reprecipitation (11, 31, 32). Work on carbonatites of diverse ages suggests that extensive reordering of ^{13}C—^{18}O bonds due to solid-state diffusion occurs at temperatures above ~250 °C, although partial bond reordering may take place at lower temperatures (33). The mineralogical composition of underlying strata indicates that the La Meseta Fm. sediments were not buried below 1 km and did not experience temperatures higher than 80 °C (34). Therefore, the La Meseta bivalve shells are unlikely to have experienced substantial reordering of carbonate bonds due to solid-state diffusion.

We tested for potential burial alteration by comparing clumped isotope temperatures of void-filling calcite cement (Fig. 3*A*),

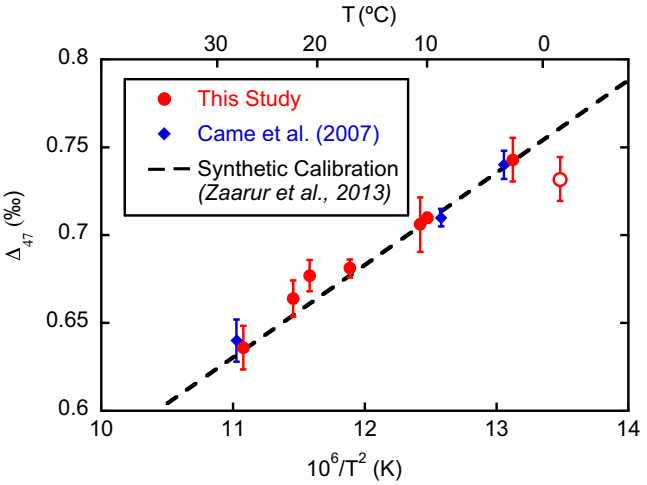

Fig. 2. Δ_{47} vs. estimated growth temperature in modern bivalve samples. Error bars indicate the analytical standard error (1σ SEM) of replicate measurements. With one exception the modern samples agree well with the Δ_{47}–T calibration based on measurements of synthetic calcite (23). The Δ_{47} value of *Laternula elliptica* (unfilled red circle) do not agree with the synthetic calcite calibration. This shell is trimineralic and includes vaterite (29), which may account for its divergent Δ_{47} value. Similar anomalously low Δ_{47} values have been observed in other cold-water taxa (28, 30).

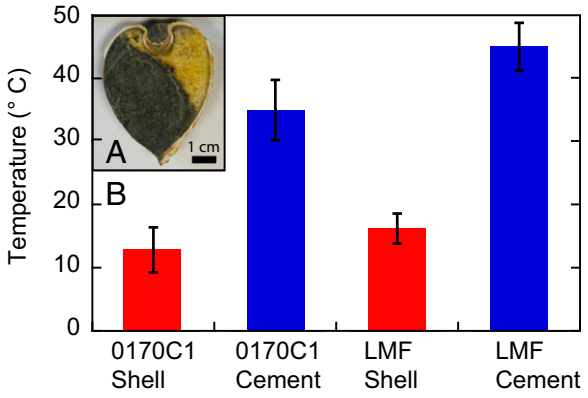

Fig. 3. (*A*) Photograph of cross-section of *Cucullaea* shell 0170C1. Calcite cement is located in the upper right interior of the shell; the darker material filling the rest of the shell is lithified sediment. (*B*) Comparison of Δ_{47}-derived temperatures for bivalve shells and co-occurring void-filling cement. Cements clearly record a higher temperature than shell carbonate, reflecting the higher temperatures during burial and indicating that temperatures recorded by bivalve shells were not substantially altered during diagenesis.

which was likely produced under burial conditions, to that of adjacent shell aragonite. Δ_{47}-derived temperatures for void-filling cements (34–43 °C) are significantly higher than the shell-derived temperatures (13–16 °C) (Fig. 3 and Table S3), and are consistent with burial at depths of ∼1 km, assuming a standard 25 °C km^{-1} geothermal gradient. Δ_{47} values in these cement-filled shells are similar to other values from La Meseta Fm. shells (Table S3), whereas the cement Δ_{47} values are clearly outside the range of all bivalve shell measurements (Fig. 3*B*). The observation that conditions associated with precipitation of secondary calcite did not overprint shell Δ_{47} values implies that shell exposure to burial temperatures at least as high as 43 °C did not lead to major alteration due to solid-state diffusion. Sensitivity analyses for the effects of solid-state diffusion and alteration due to overgrowth or recrystallization (*SI Text*) suggest that, given reasonable assumptions for burial temperature and the extent of carbonate-bond resetting, a diagenetic shift in shell Δ_{47} values is unlikely to have exceeded 0.011‰. This change in Δ_{47} is equivalent to a temperature difference of 2.5 °C, and is within the typical analytical error of clumped isotope measurements (Table S3). Given the potential for diagenetic alteration to lead to slightly elevated Δ_{47}-derived temperatures, however, the Δ_{47}-derived temperatures represent an upper bound on Seymour Island SSTs, and the inferred zonal SST gradient between the southwest Pacific and South Atlantic discussed below is therefore a minimum estimate.

La Meseta Fm. Paleotemperature Data. Bivalve Δ_{47} data record benthic temperatures and are equivalent to SST in the shallow, well-mixed setting of the La Meseta Fm. (11). Most Δ_{47} temperature estimates from the La Meseta Fm. bivalves range from 10 to 17 °C (1σ SD; Fig. 4*A*). Seasonally resolved oxygen-isotope measurements (11, 12) suggest that bulk *Eurhomalea*-derived paleotemperatures approximate mean annual SSTs, and *Cucullaea*-derived temperatures are slightly biased to the austral winter

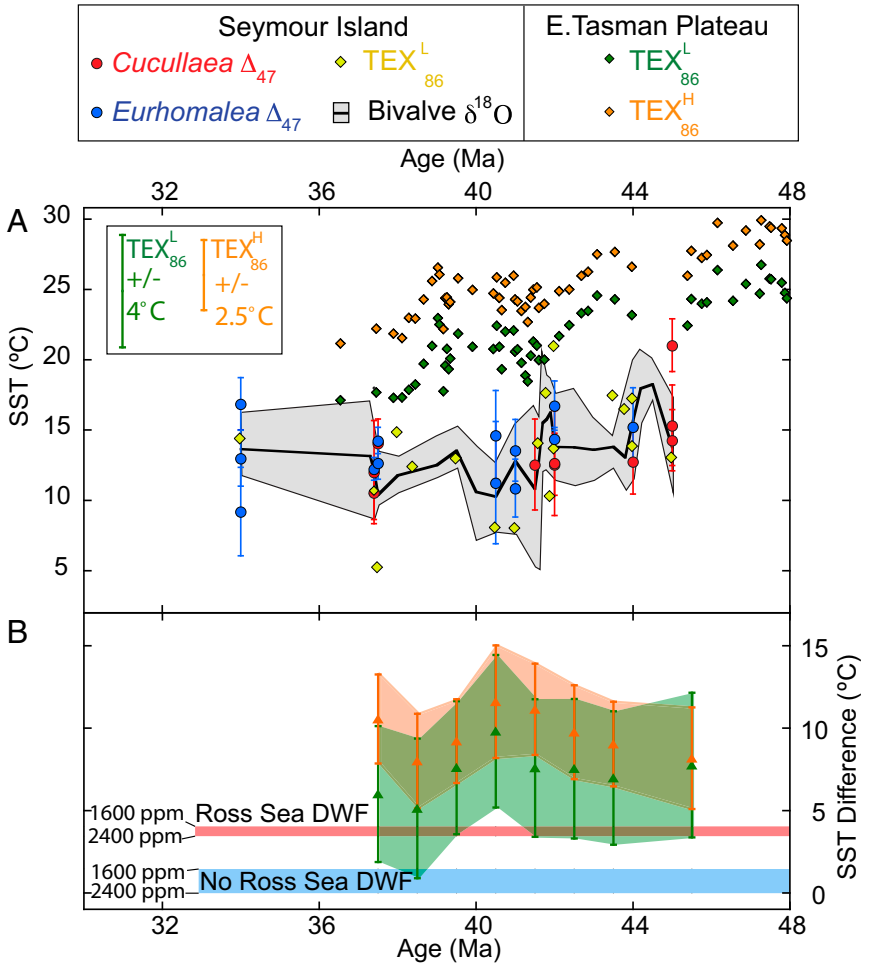

Fig. 4. (*A*) SST estimates from the Seymour Island La Meseta Fm. and the East Tasman Plateau (ODP site 1172). Error bars for Δ_{47} measurements depict analytical uncertainty (typically ±2–4 °C SEM). Calibration error for TEX^H_{86} and TEX^L_{86} (9) are indicated in the legend. $\delta^{18}O$-derived temperature estimates are calculated using $\delta^{18}O_w$ values calculated from clumped isotope derived temperatures (Fig. S2 and *SI Text*); the black line depicts the mean $\delta^{18}O$-derived temperature and the gray band indicates the range of all values. (*B*) Temperature differences between Seymour Island and the East Tasman Plateau, as derived from either proxy data or model output. Data points depict differences between East Tasman Plateau temperatures (TEX^L_{86}, green; TEX^H_{86}, orange) (7) and Seymour Island multiproxy (Δ_{47} and TEX^L_{86}) temperatures. The plotted error bars indicate the combination of the SEM of binned paleotemperatures and the calibration error for TEX^H_{86} and TEX^L_{86}. The red and blue bands indicate the range of SST differences in the UVic climate model simulations with and without deep-water formation (DWF) in the Ross Sea, respectively. See text for details.

(*SI Text*). Δ_{47} temperatures are generally 1–5 °C warmer than previous $\delta^{18}O$ estimates (11) due to uncertainty in the previously assumed oxygen-isotope composition of local seawater ($\delta^{18}O_w$). Coupled analyses of bivalve shell $\delta^{18}O$ and Δ_{47} suggest that local $\delta^{18}O_w$, although variable, averages −1.2‰ (Fig. S2). A brief excursion to $\delta^{18}O_w$ values as low as −3‰ around 41 Ma is likely associated with freshwater influx. Latest-middle and late-Eocene $\delta^{18}O_w$ values are slightly more positive than those lower in the section, suggesting an increase in salinity or the potential for minor ice growth.

We compare bivalve Δ_{47} paleotemperatures to those derived from the distribution of archaeal lipids (TEX_{86}). There are multiple calibrations relating TEX_{86} to SST (9), and it is uncertain which is most relevant to Eocene high-latitude SSTs. Clumped isotope paleotemperature estimates below 15 °C, the subpolar location of Seymour Island, and the shallow-water environment of the La Meseta Fm. all provide justification for the use of the TEX_{86}^{L} calibration (4, 9, 35) (*SI Text*). La Meseta Fm. TEX_{86}^{L} temperatures between 9 and 17 °C (1σ SD) generally agree with bivalve Δ_{47} SST estimates (Fig. 4*A* and Table S4). Many of the La Meseta Fm. sediment samples contain a relatively high proportion of soil organic matter as inferred from the branched and isoprenoid tetraether (BIT) index (14, 36), but we find no evidence that this biases TEX_{86}^{L} temperature estimates (Fig. S3*A* and *SI Text*). The BIT index is not significantly correlated with TEX_{86}^{L} values and application of the TEX_{86}' temperature calibration, which was specifically developed for sites with high BIT values (37), results in similar paleotemperatures to the TEX_{86}^{L} calibration (Table S4).

Evidence for Zonal SST Heterogeneity. Middle- and late-Eocene multiproxy SST estimates from Seymour Island are on average 7 °C cooler than TEX_{86}^{L}-derived temperatures from the East Tasman Plateau (7) (Fig. 4), despite similar latitudinal positions (Fig. 1). A recent study concluded that TEX_{86}^{L} is the preferred calibration at the East Tasman Plateau (4), but agreement between middle Eocene TEX_{86}^{H} and $U_{37}^{k'}$ SST estimates (7, 38) complicate this assessment (Fig. S3). It is possible that seasonality in alkenone production or diagenetic alteration partially account for $U_{37}^{k'}$ providing warmer SST estimates than TEX_{86}^{L} at this site (*SI Text*). If TEX_{86}^{H} is applied at the East Tasman Plateau, the temperature difference with Seymour Island increases to ∼10 °C (Fig. 4*B*). Despite uncertainty in the choice of TEX_{86} calibration, records based on other temperature proxies confirm that southwest Pacific SSTs were above 17 °C for most of the Eocene (4, 8, 16, 38) (Fig. S3). These results confirm a substantial middle-to-late Eocene temperature difference between Seymour Island and the East Tasman Plateau, reflecting a large-scale zonal SST gradient between the South Atlantic and the southwest Pacific.

Mechanisms for Zonal SST Gradients. To assess possible mechanisms responsible for the observed zonal SST gradient, we compared SST proxy records with climate simulations from the University of Victoria (UVic) intermediate complexity coupled model run with Eocene paleogeography and atmospheric pCO_2 of either 1,600 or 2,400 ppm (39). We focus on simulations in which the Tasman Gateway is closed to deep flow, consistent with evidence for deep opening of the Tasman Gateway only after ∼35.5 Ma (40). There is evidence for shallow flow across the Tasman Gateway during the middle and late Eocene (40, 41), but given the vertical resolution of the UVic model, a closed Tasman Gateway is the most appropriate paleogeography for modeling this time interval (*SI Text*). With these boundary conditions, the UVic model predicts deep-water formation in the Ross Sea (Fig. 1) and simulates SSTs at the East Tasman Plateau that are 3.5–4 °C warmer than at Seymour Island (Figs. 1 and 4*B*, Fig. S4). In a set of model simulations where deep-water formation in the Ross Sea is suppressed, however, the SST gradient between the East Tasman Plateau and Seymour Island is reduced to 0–1.5 °C (Fig. 4*B* and Fig. S4). This difference in modeled SST gradients suggests that Ross Sea deep-water formation is a critical factor that accounts for much of the observed temperature difference between the southwest Pacific and South Atlantic.

In the UVic model simulations, deep-water formation in the Ross Sea is associated with enhanced ocean heat transport in the South Pacific (39) (Fig. S5), leading to warmer SSTs relative to the South Atlantic at a given latitude (Fig. 1). Modeled deep-water formation primarily occurs in the Ross Sea due to high salinity, despite cooler SSTs in the South Atlantic. Deep sinking along the southern flank of the proto-Ross gyre (Fig. 1) enhances the efficiency of this gyre in transporting warm water from its subtropical northern flank to the subpolar South Pacific (Fig. S5). Enhanced ocean heat transport in the South Pacific is a general result of net poleward flow at the surface and net equatorward flow at depth, and is not dependent on specific transport pathways for warm surface waters. Notably, the UVic model predicts northward flow at the East Tasman Plateau, and southeastward flow to the east transports subtropical waters toward New Zealand (Fig. 1). This modeled paleocirculation is consistent with Eocene plankton biogeographic data indicating Antarctic-derived assemblages at the East Tasman Plateau (42), and a greater proportion of subtropical taxa near New Zealand (42, 43).

Eocene deep-water formation in the South Pacific is supported by neodymium isotope measurements of benthic foraminifera (44, 45). Additionally, the strong correlation between East Tasman Plateau TEX_{86} and global benthic foraminifera $\delta^{18}O$ records suggest that bottom-water formation took place near the East Tasman Plateau (7). Enhanced oceanic heat transport to the southwest Pacific is supported by relatively high middle-and-late Eocene SST estimates at the East Tasman Plateau (7), Deep Sea Drilling Program (DSDP) site 277 (16), and New Zealand (4, 8, 46) (Fig. 5 and Fig. S3). Conversely, relatively cool SSTs are

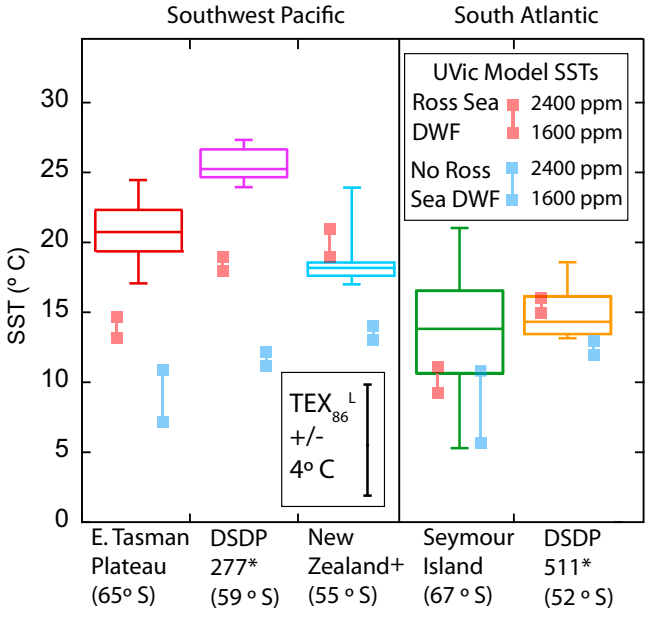

Fig. 5. Comparison of TEX_{86}^{L} and model SSTs for the middle and late Eocene southwest Pacific and South Atlantic. Boxplots indicate the distribution of TEX_{86}^{L} SST estimates from stratigraphic horizons dated to 45 Ma or younger (Fig. S5). The top, center, and bottom of the boxes indicate the upper quartile, median, and lower quartile values, respectively; the outer bars indicate maximum and minimum values; + and * indicate that only middle or late Eocene data are available for the indicated sites, respectively. Red and blue squares indicate UVic model site-specific annual SSTs under different DWF and pCO_2 scenarios.

recorded in the South Atlantic at DSDP site 511 (16), in addition to Seymour Island (Fig. 5 and Fig. S3). UVic model simulations with deep-water formation in the Ross Sea provide a much better fit to the observed distribution of proxy SSTs in the southwest Pacific and South Atlantic relative to simulations in which Ross Sea deep-water formation is suppressed (Fig. 5). UVic model SSTs are in good agreement with proxy data from New Zealand, Seymour Island and DSDP 511, but are still 6–8 °C cooler than median TEX_{86}^{L} SSTs at the East Tasman Plateau and DSDP 277 (Fig. 5).

The remaining differences between modeled and proxy SST estimates at the East Tasman Plateau and DSDP 277 may be due to atmospheric feedbacks to warm high-latitude ocean temperatures that are not represented in the intermediate complexity UVic model, such as high-latitude convective clouds (5) or enhanced atmospheric latent-heat transport associated with an intensified hydrologic cycle (47). Such feedbacks are likely to have had an enhanced effect in the southwest Pacific relative to the South Atlantic given the warmer regional SSTs. Additionally, southward extension of the proto-East Australian Current (EAC) has previously been proposed as an effective mechanism for generating elevated SSTs at the East Tasman Plateau (4, 39). However, this hypothesis is inconsistent with biogeographical data from the East Tasman Plateau that indicate an Antarctic-derived surface current at that site and do not support a large input of subtropical water (21, 42). Although southward extension of the proto-EAC in the Eocene remains uncertain, such a phenomenon may be consistent with evidence for a poleward shift and intensification of subtropical western boundary currents under current global warming (48).

Relatively cool model temperatures in the South Atlantic result from the absence of thermohaline-driven ocean heat transport in the proto-Weddell gyre, as well as greater heat loss across its southern flank due to its longer trajectory along the Antarctic continent (Fig. 1). It is possible that a westward Antarctic countercurrent, which could have formed due to shallow throughflow across the Tasman Gateway beginning around ∼49 Ma (40, 41), further cooled the proto-Weddell gyre by disrupting the input of subtropical waters to the Australo-Antarctic Gulf.

Eocene High-Latitude Temperature Distributions. Middle- and late-Eocene SST reconstructions from Seymour Island agree with modeled site-specific annual SSTs (10–15 °C) in several recent fully coupled Paleogene climate simulations with moderate to high pCO_2 values (1,120–4,480 ppm) (2, 3, 49–51). This data–model agreement contrasts with data–model discrepancies in the southwest Pacific (4, 7, 8), where middle-Eocene SST estimates are 5–15 °C warmer than SSTs in all models (2). We suggest that oceanic heat transport driven by deep-water formation in the Ross Sea partially explains high SSTs in the southwest Pacific, and that these high SST estimates are not representative of zonal-mean Eocene high-latitude ocean temperatures. Likewise, cool SSTs at Seymour Island imply that the South Atlantic was one of the coldest marine environments in the Southern Hemisphere during the middle and late Eocene. These results suggest that high-latitude warming under elevated atmospheric greenhouse gas concentrations can exhibit large-scale zonal variability, with higher temperatures potentially concentrated in regions of deep-water formation.

Materials and Methods

Palynological Analysis. Eight sediment samples (Table S1) were spiked with an exote and treated with 10% and 30% HCl and 40% HF solutions for carbonate and silica removal. Disaggregated palynological residues were analyzed at 200–1,000× magnification. Palynological classification was performed using the taxonomy of refs. 52 and 53.

La Meseta Fm. Bivalve Shell Sampling. Nineteen shells from two bivalve genera (*Cucullaea* and *Eurhomalea*) from horizons spanning the Tertiary Eocene La Meseta stratigraphic units 2–7 (11) were selected for clumped isotope analysis (Table S3). Shells were sampled at their interior cross-sections where possible. Where surface sampling was necessary, the outermost shell material was removed and samples were collected from shell interiors. In two samples we also sampled calcite cement 1 cm away from the inner shell surface (Fig. 3*A*).

Modern Bivalve Shell Sampling. To test the Δ_{47}–temperature relationship in bivalve carbonate we analyzed the shells of eight modern shallow-water coastal bivalves of different taxa with widely varying growth temperatures (Table S2). Growth temperature estimates for each bivalve shell were derived from Simple Ocean Data Assimilation (SODA) SST reanalysis data from 1980 to 2007 (10). Estimates of growth seasonality are derived, where available, from ontogenetic or stable isotope studies of shell growth in the taxa studied (54–58) (Table S2). For taxa in which the growing season is not well known we either applied the mean temperature of the six warmest months (for temperate taxa) (24), or mean annual temperature (for an equatorial taxon). Most of the studied shells are aragonitic, but the *Crassostrea* specimen is calcitic, the *Mytilus* specimen contains calcite and aragonite, and the *Laternula* specimen contains calcite, aragonite, and vaterite (29) (Table S2).

Clumped Isotope Analyses. Carbonate clumped isotope analyses were conducted at Yale University, as described previously (23). Aliquots of bivalve shell carbonate were reacted with 103% phosphoric acid overnight at 25 °C. The resulting CO_2 was collected cryogenically followed by trapping volatile organic molecules using a GC column (Supelco Supel-Q PLOT; 30 m × 0.53 mm) cooled to −20 °C (15, 59). The CO_2 was then analyzed for $\delta^{13}C$, $\delta^{18}O$, and Δ_{47} by a Thermo-Finnigan MAT-253 isotope ratio mass spectrometer configured to measure masses 44–49 (60). Samples were measured in five batches over 22 months (January 2009 to November 2011) to avoid errors associated with short-term fluctuations in mass-spectrometric and sample preparation parameters. Between one and nine replicate analyses were conducted per sample (Tables S2 and S3). Δ_{47} values are defined relative to CO_2 heated to 1,000 °C, which has a nearly stochastic distribution of isotopologues (Δ_{47} = 0.027‰; ref. 61). Δ_{47} values are presented in both the original laboratory reference frame, as well as an absolute reference frame based on the analysis of standards calibrated through interlaboratory comparison (62). The long-term precision of the Carrera marble carbonate standard is 0.029‰ (1σ SD). The typical precision for abiogenic carbonates on this mass spectrometer is 0.020‰ (23). The mean Δ_{47} value of Carrera marble measured during the period of sample analysis was 0.403‰ (absolute reference frame), within error of the established value for Yale University (0.400‰; ref. 62). Temperatures were calculated from Δ_{47} values using the calibration of ref. 23 (*SI Text*).

La Meseta Fm. Sedimentary Glycerol Dibiphytanyl Glycerol Tetraether Lipid Analyses. Eighteen sediment samples from the La Meseta Fm. were analyzed for glycerol dibiphytanyl glycerol tetraether (GDGT) distributions at either Yale University or Utrecht University and the Royal Netherlands Institute for Sea Research (NIOZ) (Table S4) using methodology described previously (9, 16). Freeze-dried sediment samples were extracted with a Soxhlet extractor using either a 2:1 (Yale) or 1:1 (Utrecht/NIOZ) dichloromethane:methanol solvent mixture. The lipid extracts were purified with silica gel and activated alumina chromatography (Yale) or activated alumina chromatography alone (Utrecht/NIOZ). All samples were filtered through 0.45-μm glass fiber. GDGT lipids were analyzed by HPLC-mass spectrometry (Agilent 1100) using a Prevail Cyano column with 99:1 hexane:isopropanol as eluent. TEX_{86}^{L} and TEX_{86}^{H} values were calculated following ref. 9. The BIT index was calculated following ref. 36.

Calculation of Intersite SST Differences. To estimate SST differences between Seymour Island and the East Tasman Plateau (Fig. 4*B*) we binned paleotemperature estimates into 1-Ma intervals. For the East Tasman Plateau we calculated the mean TEX_{86}^{L}- or TEX_{86}^{H}-derived temperature for each interval. For Seymour Island we calculated the mean of all TEX_{86}^{L}- and Δ_{47}-derived temperatures (Tables S3 and S4). Temperature differences are calculated as the difference in the mean temperature between the two sites for each interval.

UVic Climate Model Simulations. The climate model simulations discussed in this paper use the UVic model, a modified and enhanced version of the intermediate-complexity coupled model described in detail in ref. 63. We applied the late Eocene bathymetry, topography, and vegetation used by ref. 42. The model geography is slightly modified from that of ref. 42 in that Australia is located 4.5° farther to the south. Model parameters are described in detail in ref. 39. To examine the effect of DWF in the Ross Sea on general circulation, we conducted simulations where additional fresh water is added to the Ross Sea to suppress DWF there (Fig. S4), as described in ref. 39.

ACKNOWLEDGMENTS. Gerard Olack, Dominic Colosi, and Glendon Hunsinger provided assistance with clumped isotope measurements; Shikma Zaarur

provided advice on clumped isotope data analysis; Christy Visaggi, Michelle Casey, and Steven Roof provided modern bivalve samples; and Natasja Welters and Jan van Tongeren (Utrecht University) assisted with palynological preparations. We thank two anonymous reviewers for constructive commentary. This work was supported by US National Science Foundation Grants EAR-0842482 (to H.P.A.) and PLR-0125409 (to L.C.I.), and Statoil and European Research Council Starting Grant 259627 (to A.S.).

1. Zachos JC, Dickens GR, Zeebe RE (2008) An early Cenozoic perspective on greenhouse warming and carbon-cycle dynamics. *Nature* 451(7176):279–283.
2. Lunt DJ, et al. (2012) A model–data comparison for a multi-model ensemble of early Eocene atmosphere–ocean simulations: EoMIP. *Clim Past* 8(5):1717–1736.
3. Huber M, Caballero R (2011) The early Eocene equable climate problem revisited. *Clim Past* 7(2):603–633.
4. Hollis CJ, et al. (2012) Early Paleogene temperature history of the Southwest Pacific Ocean: Reconciling proxies and models. *Earth Planet Sci Lett* 349-350:53–66.
5. Abbot DS, Tziperman E (2008) A high-latitude convective cloud feedback and equable climates. *Q J R Meteorol Soc* 134(630):165–185.
6. Sloan LC, Pollard D (1998) Polar stratospheric clouds: A high latitude warming mechanism in an ancient greenhouse world. *Geophys Res Lett* 25(18):3517–3520.
7. Bijl PK, et al. (2009) Early Palaeogene temperature evolution of the southwest Pacific Ocean. *Nature* 461(7265):776–779.
8. Hollis CJ, et al. (2009) Tropical sea temperatures in the high-latitude South Pacific during the Eocene. *Geology* 37(2):99–102.
9. Kim JH, et al. (2010) New indices and calibrations derived from the distribution of crenarchaeal isoprenoid tetraether lipids: Implications for past sea surface temperature reconstructions. *Geochim Cosmochim Acta* 74(16):4639–4654.
10. Carton JA, Giese BS (2008) A reanalysis of ocean climate using Simple Ocean Data Assimilation (SODA). *Mon Weather Rev* 136(8):2999–3017.
11. Ivany LC, et al. (2008) Eocene climate record of a high southern latitude continental shelf: Seymour Island, Antarctica. *Geol Soc Am Bull* 120(5-6):659–678.
12. Dutton AL, Lohmann KC, Zinsmeister WJ (2002) Stable isotope and minor element proxies for Eocene climate of Seymour Island, Antarctica. *Paleoceanography* 17(2): PA0593.
13. Shah SR, Mollenhauer G, Ohkouchi N, Eglinton TI, Pearson A (2008) Origins of archaeal tetraether lipids in sediments: Insights from radiocarbon analysis. *Geochim Cosmochim Acta* 72(18):4577–4594.
14. Schouten S, Hopmans EC, Sinninghe Damsté JS (2013) The organic geochemistry of glycerol dialkyl glycerol tetraether lipids: A review. *Org Geochem* 54:19–61.
15. Ghosh P, et al. (2006) ^{13}C-^{18}O bonds in carbonate minerals: A new kind of paleothermometer. *Geochim Cosmochim Acta* 70(6):1439–1456.
16. Liu ZH, et al. (2009) Global cooling during the Eocene-Oligocene climate transition. *Science* 323(5918):1187–1190.
17. Bijl PK, Sluijs A, Brinkhuis H (2013) A magneto- and chemostratigraphically calibrated dinoflagellate cyst zonation of the early Palaeogene South Pacific Ocean. *Earth Sci Rev* 124:1–31.
18. Vandenberghe N, Speijer RP, Hilgen FJ (2012) The Paleogene period. *The Geologic Time Scale 2012*, eds Gradstein FM, Ogg JG, Schmitz M, Ogg G (Elsevier, Amsterdam), pp 855–922.
19. Brinkhuis H, Sengers S, Sluijs A, Warnaar J, Williams GL (2003) Latest Cretaceous-earliest Oligocene and Quaternary dinoflagellate cysts, ODP site 1172, East Tasman Plateau. *Proceedings of the Ocean Drilling Program, Scientific Results*, eds Exon, NF Kennett JP, Malone MJ, Vol 189. Available at www-odp.tamu.edu/publications/189_SR/106/106.htm. Accessed April 7, 2014.
20. Williams GL, Brinkhuis HMAP, Fensome RA, Weegink JW (2004) Southern Ocean and global dinoflagellate cyst events compared: Index events for the Late Cretaceous - Neogene. *Proceedings of the Ocean Drilling Program, Scientific Results*, eds Exon NF, Kennett JP, Malone MJ, Vol 189. Available at www-odp.tamu.edu/publications/189_SR/107/107.htm. Accessed April 7, 2014.
21. Bijl PK, et al. (2011) Environmental forcings of Paleogene Southern Ocean dinoflagellate biogeography. *Paleoceanography* 26(1).
22. McArthur JM, Howarth RJ, Bailey TR (2001) Strontium isotope stratigraphy: LOWESS version 3: Best fit to the marine Sr-isotope curve for 0-509 Ma and accompanying look-up table for deriving numerical age. *J Geol* 109(2):155–170.
23. Zaarur S, Affek HP, Brandon MT (2013) A revised calibration of the clumped isotope thermometer. *Earth Planet Sci Lett* 382:47–57.
24. Came RE, et al. (2007) Coupling of surface temperatures and atmospheric CO_2 concentrations during the Palaeozoic era. *Nature* 449(7159):198–201.
25. Hren MT, et al. (2013) Terrestrial cooling in Northern Europe during the Eocene–Oligocene transition. *Proc Natl Acad Sci USA* 110(19):7562–7567.
26. Dennis K, Cochran J, Landman N, Schrag D (2013) The climate of the Late Cretaceous: New insights from the application of the carbonate clumped isotope thermometer to Western Interior Seaway macrofossil. *Earth Planet Sci Lett* 362:51–65.
27. Henkes GA, et al. (2013) Carbonate clumped isotope compositions of modern marine mollusk and brachiopod shells. *Geochim Cosmochim Acta* 106:307–325.
28. Eagle RA, et al. (2013) The influence of temperature and seawater carbonate saturation state on ^{13}C–^{18}O bond ordering in bivalve mollusks. *Biogeosciences* 10(7): 4591–4606.
29. Nehrke G, Poigner H, Wilhelms-Dick D, Brey T, Abele D (2012) Coexistence of three calcium carbonate polymorphs in the shell of the Antarctic clam Laternula elliptica. *Geochem Geophy Geosy* 13(5):Q05014.
30. Tripati AK, et al. (2010) ^{13}C-^{18}O isotope signatures and 'clumped isotope' thermometry in foraminifera and coccoliths. *Geochim Cosmochim Acta* 74(20):5697–5717.
31. Buick DP, Ivany LC (2004) 100 years in the dark: Extreme longevity of Eocene bivalves from Antarctica. *Geology* 32(10):921–924.
32. Ivany LC, Runnegar B (2010) Early Permian seasonality from bivalve $\delta^{18}O$ and implications for the oxygen isotopic composition of seawater. *Geology* 38(11):1027–1030.
33. Dennis KJ, Schrag DP (2010) Clumped isotope thermometry of carbonatites as an indicator of diagenetic alteration. *Geochim Cosmochim Acta* 74(14):4110–4122.
34. Pirrie D, Ditchfield PW, Marshall JD (1994) Burial diagenesis and pore-fluid evolution in a Mesozoic back-arc basin - The Marambio Group, Vega Island, Antarctica. *J Sediment Res A* 64(3):541–552.
35. Taylor KW, Huber M, Hollis CJ, Hernandez-Sanchez MT, Pancost RD (2013) Re-evaluating modern and Palaeogene GDGT distributions: Implications for SST reconstructions. *Global Planet Change* 108:158–174.
36. Hopmans EC, et al. (2004) A novel proxy for terrestrial organic matter in sediments based on branched and isoprenoid tetraether lipids. *Earth Planet Sci Lett* 224(1-2): 107–116.
37. Sluijs A, et al.; Expedition 302 Scientists (2006) Subtropical Arctic Ocean temperatures during the Palaeocene/Eocene thermal maximum. *Nature* 441(7093):610–613.
38. Bijl PK, et al. (2010) Transient Middle Eocene atmospheric CO_2 and temperature variations. *Science* 330(6005):819–821.
39. Sijp WP, England MH, Huber M (2011) Effect of the deepening of the Tasman Gateway on the global ocean. *Paleoceanography* 26:PA4207.
40. Stickley CE, et al. (2004) Timing and nature of the deepening of the Tasmanian Gateway. *Paleoceanography* 19(4):PA4027.
41. Bijl PK, et al.; Expedition 318 Scientists (2013) Eocene cooling linked to early flow across the Tasmanian Gateway. *Proc Natl Acad Sci USA* 110(24):9645–9650.
42. Huber M, et al. (2004) Eocene circulation of the Southern Ocean: Was Antarctica kept warm by subtropical waters? *Paleoceanography* 19(4):PA4026.
43. Kennett JP, Exon NF (2004) Paleoceanographic evolution of the Tasmanian Seaway and its climatic implications. *Geophys Monogr Ser* 151:345–367.
44. Thomas DJ (2004) Evidence for deep-water production in the North Pacific Ocean during the early Cenozoic warm interval. *Nature* 430(6995):65–68.
45. Hague AM, et al. (2012) Convection of North Pacific deep water during the early Cenozoic. *Geology* 40(6):527–530.
46. Burgess CE, et al. (2008) Middle Eocene climate cyclicity in the southern Pacific: Implications for global ice volume. *Geology* 36(8):651–654.
47. Durack PJ, Wijffels SE, Matear RJ (2012) Ocean salinities reveal strong global water cycle intensification during 1950 to 2000. *Science* 336(6080):455–458.
48. Wu L, et al. (2012) Enhanced warming over the global subtropical western boundary currents. *Nature Climate Change* 2(3):161–166.
49. Roberts CD, LeGrande AN, Tripati AK (2009) Climate sensitivity to Arctic seaway restriction during the early Paleogene. *Earth Planet Sci Lett* 286(3-4):576–585.
50. Lunt DJ, et al. (2010) CO_2-driven ocean circulation changes as an amplifier of Paleocene-Eocene thermal maximum hydrate destabilization. *Geology* 38(10):875–878.
51. Winguth A, Shellito C, Shields C, Winguth C (2010) Climate response at the Paleocene–Eocene thermal maximum to greenhouse gas forcing—A model study with CCSM3. *J Clim* 23(10):2562–2584.
52. Fensome RA, Williams GL, MacRae RA (2009) Late Cretaceous and Cenozoic fossil dinoflagellates and other palynomorphs from the Scotian Margin, offshore eastern Canada. *J Syst Palaeontol* 7(1):1–79.
53. Sluijs A, Brinkhuis H, Williams GL, Fensome RA (2009) Taxonomic revision of some Cretaceous-Cenozoic spiny organic-walled peridiniacean dinoflagellate cysts. *Rev Palaeobot Palynol* 154(1-4):34–53.
54. Dame RF (1976) Energy-flow in an intertidal oyster population. *Estuar Coast Mar Sci* 4(3):243–253.
55. Hilbish TJ (1986) Growth trajectories of shell and soft-tissue in bivalves - Seasonal-variation in *Mytilus edulis L*. *J Exp Mar Biol Ecol* 96(2):103–113.
56. Quitmyer IR, Jones DS, Arnold WS (1997) The sclerochronology of hard clams, Mercenaria spp., from the south-eastern USA: A method of elucidating the zooarchaeological records of seasonal resource procurement and seasonality in prehistoric shell middens. *J Archaeol Sci* 24(9):825–840.
57. Ivany LC, Wilkinson BH, Jones DS (2003) Using stable isotopic data to resolve rate and duration of growth throughout ontogeny: An example from the surf clam, *Spisula solidissima*. *Palaios* 18(2):126–137.
58. Brey T, Mackensen A (1997) Stable isotopes prove shell growth bands in the Antarctic bivalve *Laternula elliptica* to be formed annually. *Polar Biol* 17(5):465–468.
59. Affek HP, Eiler JM (2006) Abundance of mass 47 CO_2 in urban air, car exhaust, and human breath. *Geochim Cosmochim Acta* 70(1):1–12.
60. Eiler JM, Schauble EA (2004) ^{18}O-^{13}C-^{16}O in Earth's atmosphere. *Geochim Cosmochim Acta* 68(23):4767–4777.
61. Wang ZG, Schauble EA, Eiler JM (2004) Equilibrium thermodynamics of multiply substituted isotopologues of molecular gases. *Geochim Cosmochim Acta* 68(23): 4779–4797.
62. Dennis KJ, Affek HP, Passey BH, Schrag DP, Eiler JM (2011) Defining an absolute reference frame for 'clumped' isotope studies of CO_2. *Geochim Cosmochim Acta* 75(22):7117–7131.
63. Weaver AJ, et al. (2001) The UVic Earth System Climate Model: Model description, climatology, and applications to past, present and future climates. *Atmos-ocean* 39(4):361–428.